

pubs.acs.org/acsaelm Forum Article

A Study on Contact Resistance as a Function of Surface Treatment in Perovskite Field-Effect Transistors

Colin Tyznik, Matthew Waldrip, Ryan P. Sullivan, Motahhare Mirhosseini, Adam Berry, Sean Dwyer, Hurriyet Yuce Cakir, Tonya Coffey, Yueh-Lin Loo, and Oana D. Jurchescu*

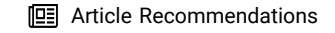


Cite This: https://doi.org/10.1021/acsaelm.3c00149

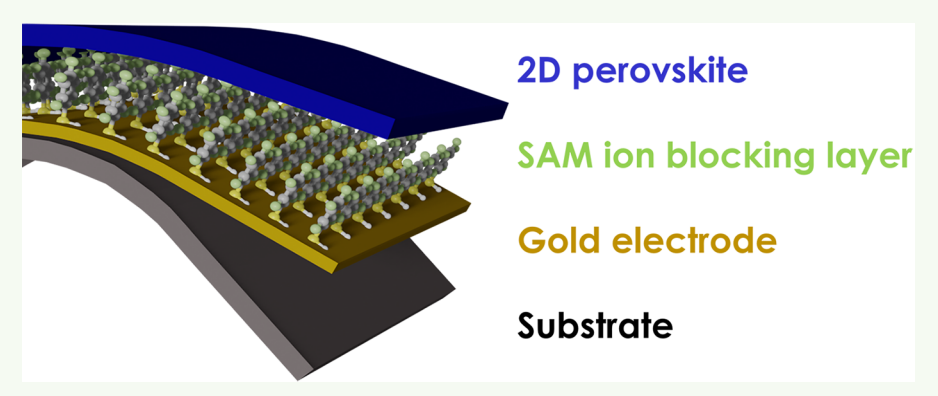


ACCESS

III Metrics & More



SI Supporting Information



ABSTRACT: Metal halide perovskites are versatile materials which have already demonstrated exceptional performance in diverse optoelectronic devices. The progress has been significant; however, the fundamental understanding of the physics of charge injection remains elusive, impeding further advancements. Here, we use field-effect transistors (FETs) to investigate the impact of surface functionalization on the charge injection and transport in thin films of phenethylammonium tin iodide (PEA₂SnI₄). We show that self-assembled monolayers (SAMs) can both assist in reducing the Schottky barrier and act as an ion blocking layer between the contact and the perovskite film, limiting interfacial chemical reactions. Consequently, the contact resistance is lowered by more than 3 times compared to untreated contacts. The temperature dependence of the charge carrier mobility is discussed considering the contributions from the channel and contacts, respectively. Our results provide a quantitative framework for the charge injection in metal halide perovskites and will contribute toward the progress of high-performance optoelectronic devices including solar cells, light-emitting diodes, as well as X-ray and photodetectors.

KEYWORDS: perovskite FETs, contact resistance, mobility, transistors, charge injection

■ INTRODUCTION

Metal halide perovskites (MHPs) are a remarkable class of materials owing to their unique and intriguing properties that have led to exceptional performance when incorporated in optoelectronic devices, such as photovoltaic cells, ¹⁻⁴ X-ray and photodetectors, ^{5,6} light-emitting diodes (LEDs), ^{7,8} field-effect transistors (FETs), 9-13 memristors, 14 lasers, 15 and more. The progress in this field has been phenomenal, especially in the past decade, but several challenges need to be addressed for MHP semiconductors to become a core materials platform of the 21st century. Among these, a good understanding of the physics of charge injection in perovskite devices is still lacking. Inefficient charge collection and transfer due to the presence of Schottky barriers, carrier recombination, and chemical reactions occurring at interfaces with the electrodes can severely impact device performance, stability, and reproducibility. 16-18 One quantitative measure for the efficiency of the injection process is the contact resistance, R_{σ} and its impact

becomes even more detrimental in devices operating under high current densities, such as FETs. ¹⁹ FETs amplify electrical signals and are the basic components of many consumer electronics; a summary of the most recent advancements in perovskite FETs can be found in several reviews on this topic. ^{9–12} Along with improving the quality of the perovskite films and controlling ion motion, it is imperative to reduce R_c in order to maximize the performance of perovskite devices. ^{20–23}

Several studies examined contact resistance in perovskite FETs and found that it depends on the device geometry and

Special Issue: Halide Perovskite Materials and Devices for Energy and Electronic Applications

Received: February 3, 2023 Accepted: May 9, 2023



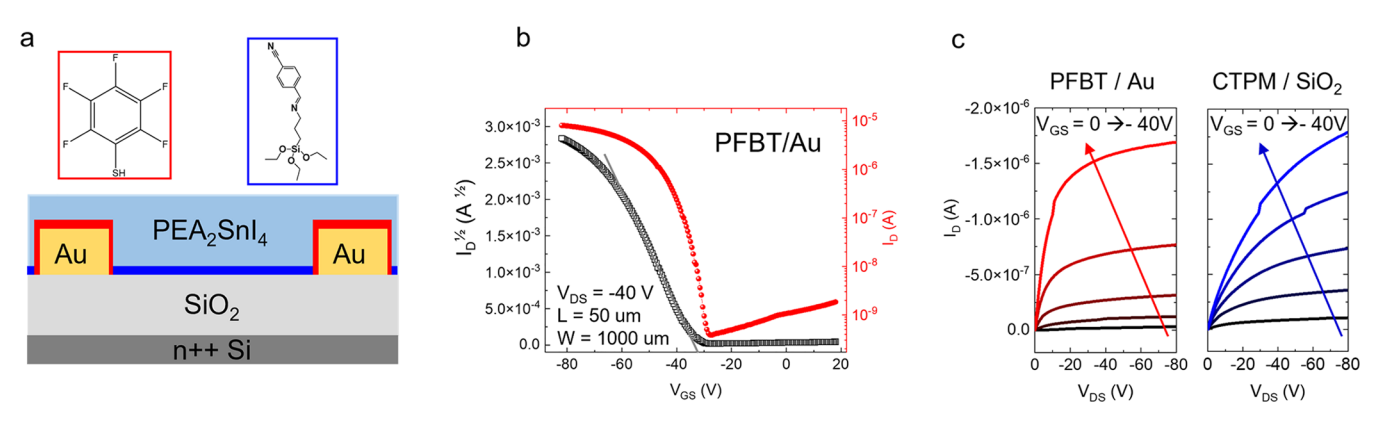


Figure 1. (a) Device architecture (side view). (b) Transfer curve of a PEA₂SnI₄ device with PFBT/Au source-drain contacts. The slope used in the mobility calculation is marked in gray. (c) Output curves for PFBT-treated contacts (red) and CTPM-treated SiO₂ (blue).

details of fabrication; $^{24-29}$ however, R_c remains understudied. Here, we addressed this challenge by investigating the impact of surface chemical functionalization and temperature on the contact resistance and charge transport in perovskite FETs. Self-assembled monolayer (SAM) treatments were applied on the dielectric and electrode surfaces, respectively, and we found that functionalization of the dielectric has little impact both on the channel properties and the contact resistance, while treatment of the Au contact reduces R, by approximately 3 times, to a value of $2.3 \times 10^4 \Omega$ cm at room temperature. This outcome results from the fact that the dense SAM positioned between the electrode and perovskite surfaces simultaneously reduces the injection barrier and creates a buffer layer, which prevents the chemical reactions that typically occur at the interface between the perovskite and Au surface, as confirmed by our elemental analysis. ^{16,30,31} We found an increase in mobility as temperature decreases due to a reduction in ionic motion screening electronic transport. We explain these results by considering the contributions of the contact and channel resistance to the overall device properties and their respective dependence on temperature due to ion migration and presence of electronic traps. Our findings provide quantitative information about the contact resistance in perovskite FETs and advance the basic understanding of processes occurring at electrode/perovskite interfaces. Given the frequent adoption of SAM treatment for interface engineering in perovskite devices, 32,33 the results obtained in this study will contribute to the progress of other perovskite optoelectronic devices including solar cells, LEDs, and X-ray and photodetectors.

■ EXPERIMENTAL SECTION

Bottom-gate, bottom-contact FETs based on phenethylammonium tin iodide (C₆H₅H₄NH₃)₂SnI₄ (PEA₂SnI₄) were fabricated and characterized. This 2D layered perovskite has been previously incorporated in transistors of various architectures and has demonstrated good performance upon careful control of the film morphology and charge injection by using surface treatments, reducing the occurrence of the process yielding Sn²⁺ oxidation to Sn⁴⁺ and defect passivation.^{34,35} Highly doped Si wafers were used as substrates and gate electrodes, and a thermally grown SiO2 film on their surfaces served as the gate dielectric. These substrates were diced in pieces of approximately 1.5 by 1.5 cm and cleaned sequentially via submersion in acetone at 85 °C, isopropyl alcohol at 85 °C, and a UV-ozone treatment for 10 min. Next, they were rinsed with deionized water (DI), dried under a nitrogen stream, and baked in air for 5 min at 155 °C. Then, rectangular electrodes were patterned using shadow masks and deposited via successive evaporation of 3 nm Ti and 40 nm Au. These substrates were cleaned again following the procedure described above before the next step. Three types of samples were fabricated: for the first type, no surface treatments have been applied; we will refer to these samples as "control". For the second type, namely the "PFBT/Au" samples, the substrates were immersed in a 30 mM solution of pentafluorobenzenethiol (PFBT) in ethanol at room temperature for 30 min after the second cleaning procedure, followed by a thorough ethanol rinse. PFBT SAM only adheres to the electrode surface via the formation of covalent Au-S bonds and not to the SiO₂. 36,37 The degree of order within this monolayer depends on the strength of this bond and the intermolecular interactions within the SAM molecules, but factors like solvent and environment can also play a role. 19 To fabricate the "CTPM/SiO₂" samples, the substrates were immersed in a 7 mM solution of (E)-1-(4-cyanophenyl)-N-(3-(triethoxysilyl)propyl)methanimine) (CTPM) in chloroform for 16 h in a nitrogen atmosphere and then rinsed with chloroform.³⁸ In this case, the SAM adheres only to the SiO₂ and not to the electrode surface.³⁹ Figure 1a displays the device architecture with two different SAM treatments, i.e., PFBT in red and CTPM in blue. The chemical formulas for the SAM molecules are also included.

To obtain the perovskite layer, a precursor was made by dissolving $C_6H_{11}NHI\$ and $\ \, SnI_2\$ in a $\ \, 2{:}1\$ ratio in methanol with a final concentration of 20 mg/mL. This precursor was deposited onto the substrates via spin coating in a glovebox under nitrogen atmosphere at 2500 rpm for 120 s. The films were then annealed at 80 $^{\circ}C$ for 10 min in the same glovebox. 34,40

Devices were patterned by scratching around the source-drain pads, and characterized using an Agilent 4155C Semiconductor Parameter Analyzer in the dark under a vacuum of at least 10^{-5} Torr and in the temperature range between 200 and 300 K. The charge carrier mobility (μ) was calculated in the saturation regime from the slope of the square root of the drain current with respect to the gate—source voltage curve, using eq 1:^{41,42}

$$I_D = \frac{W}{L} \frac{C_i}{2} \mu (V_{GS} - V_T)^2 \tag{1}$$

where L and W are the channel length and the channel width, respectively, and C_i is the capacitance per unit area of the dielectric.

Atomic force microscopy (AFM) measurements were acquired with a Bruker Icon scanning probe microscopy system in PeakForce Tapping mode using PFQNE-AL probes. These probes have a tip radius of roughly 5 nm, a spring constant of ~0.8 N/m, and a resonant frequency of ~300 kHz. All measurements were performed in ambient conditions. In PeakForce Tapping mode the cantilever oscillates off resonance, at 2000 Hz while tapping the surface. During each tap, a force curve is acquired, and the feedback loop sets the maximum force of each tap in the piconewton range to minimize sample damage and wear of the tip while determining the topography of the scan line.

Grazing incidence wide-angle X-ray scattering (GIWAXS) experiments were performed at the Complex Materials Scattering (CMS) beamline of the National Synchrotron Light Source II (NSLS-II) at

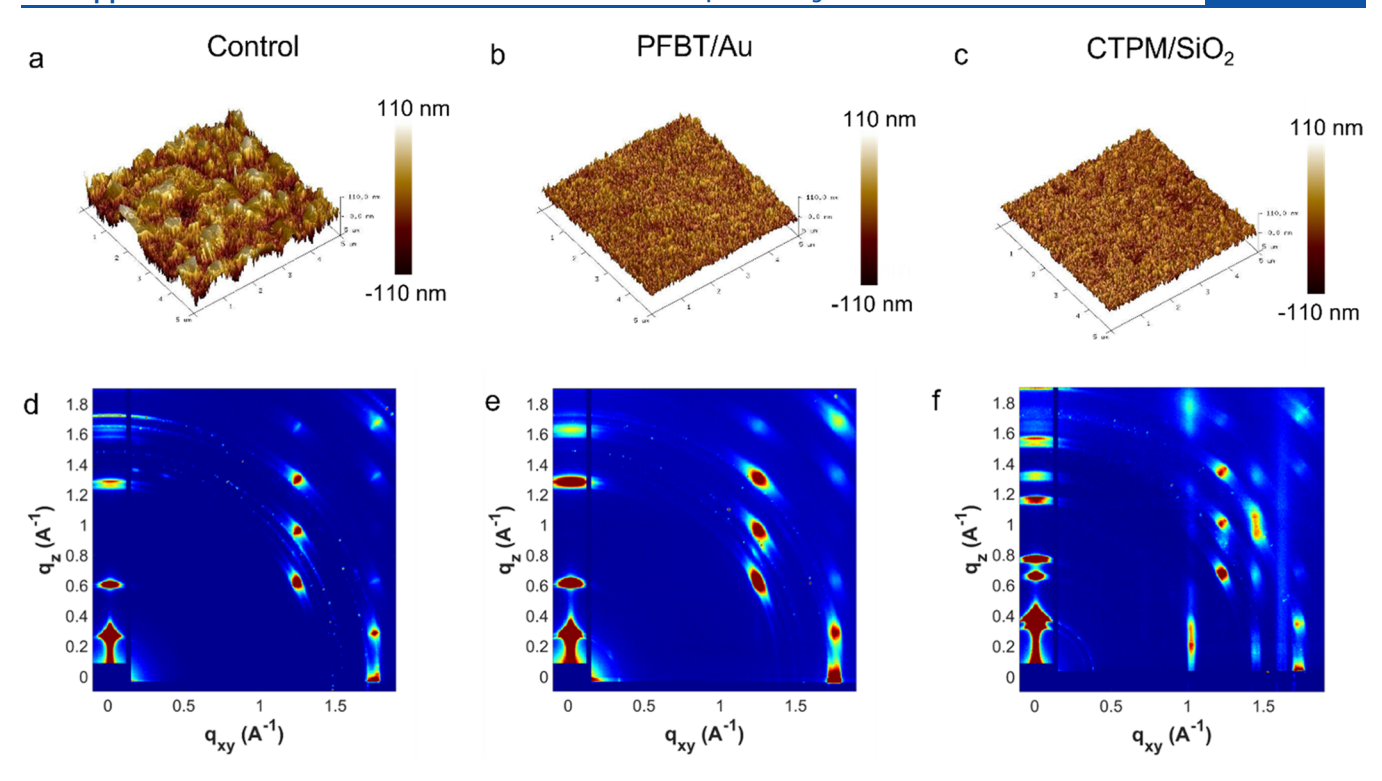


Figure 2. Analysis of film morphology. AFM measurements for (a) control, (b) PFBT-treated, and (c) CTPM/SiO₂-treated samples and GIWAX measurements for (d) control, (e) PFBT/Au, and (f) CTPM/SiO₂ samples.

the Brookhaven National Lab. The beam energy was set at $13.5~\rm keV$. GIWAXS results were collected with the incident angle of 0.15° with respect to the Si substrate. A custom-made Pilatus-800 K detector was placed at a distance of 259 mm from the sample center to capture 2D-GIWAXS images with an exposure time of 10 s. All 2D-GIWAXS images have been background subtracted.

The scanning electron microscopy (SEM) measurements and images were acquired with a JEOL JSM-IT300LV scanning electron microscope using an accelerating voltage of either 15 or 20 kV. This SEM has a lanthanum hexaboride (LaB6) filament and is equipped with an Oxford energy dispersive spectroscopy (EDS) system as well as the associated Aztec analysis software. All measurements were acquired under high vacuum (10⁻⁷-10⁻⁸ Torr). The samples were imaged in a low-current setting, and a high current was used for the Xray analysis. X-ray spectra were acquired at points of interest in the SEM images to determine the chemical composition of the samples. X-ray maps were then acquired by raster scanning the electron beam across the area of interest, generating false color X-ray images simultaneously at specific X-ray energies from the intensity of the signal at each energy. During the acquisition of the X-ray maps, the image area was scanned at least 25 times to ensure a sufficient signalto-noise ratio. These maps allowed us to see how the chemical composition of the samples varied spatially.

■ RESULTS AND DISCUSSION

Figure 1b shows a representative transfer curve of a PEA₂SnI₄ device with PFBT/Au source-drain contacts measured at room temperature; representative curves for the other sample types, as well as double-sweeps, are provided in Figures S1–S3. The two main sources of hysteresis are the ion motion and the charge trapping. The ions in the perovskite layer migrate in the presence of an electric field and create a space charge, which dominates the evolution of the current in the reverse sweep, a phenomenon that gives rise to a hysteresis in the current–voltage characteristics.²² Additionally, in Sn-based perovskites, the minority carrier trapping at iodide vacancy sites has also

been shown to contribute to the hysteresis, and the effect was reduced by cosubstitution of small amounts of bromide and chloride for iodide.³⁵ Figure 1c displays the output curves measured at room temperature for the PFBT/Au and CTPM/ SiO₂ devices. All FETs exhibited p-type field-effect transport. By investigating a large data set, we observed that the devices with treated electrodes displayed a higher current for the same FET geometry, suggesting more efficient injection and transport. Indeed, the field-effect mobility for PFBT/Au devices was $\mu = (4.5 \pm 1.5) \cdot 10^{-2} \text{ cm}^2 \text{ V}^{-1} \text{ s}^{-1}$, while the mobility of CTPM/SiO₂ devices, for which the Au contacts were not chemically modified, was $\mu = (1.4 \pm 0.8) \cdot 10^{-2} \text{ cm}^2$ V^{-1} s⁻¹. For comparison, the average mobility in control FETs with no treatments was $\mu = (9.5 \pm 1.1) \cdot 10^{-3} \text{ cm}^2 \text{ V}^{-1} \text{ s}^{-1}$. These values are lower than the best obtained in PEA2SnI4 FETs with a Cytop top-gate dielectric,³⁴ due to the higher density of trap states present at the interface with the SiO₂ dielectric compared with Cytop. 44

To understand the impact of film microstructure on the electrical properties, we investigated the perovskite thin film properties using AFM and GIWAXS. AFM measurements have been taken in the channel region of each sample type. Nevertheless, it is known that in the case of devices with chemically modified contacts, the semiconductor ordering is seeding from treated contacts, and thus, SAM treatment of the electrode surface also impacts the morphology of the film in the region between the contacts, where the channel forms. AFM measurements performed at the surface of each film type (Figure 2a-c) indicate that the perovskite film formed on untreated substrates was significantly rougher than the films formed on the treated substrates, with the root-mean-square (rms) roughness of the films on control, PFBT/Au, and CTPM/SiO₂ substrates being 33.4, 10.5, and 12.1 nm, respectively. The roughness of the films varied substantially,

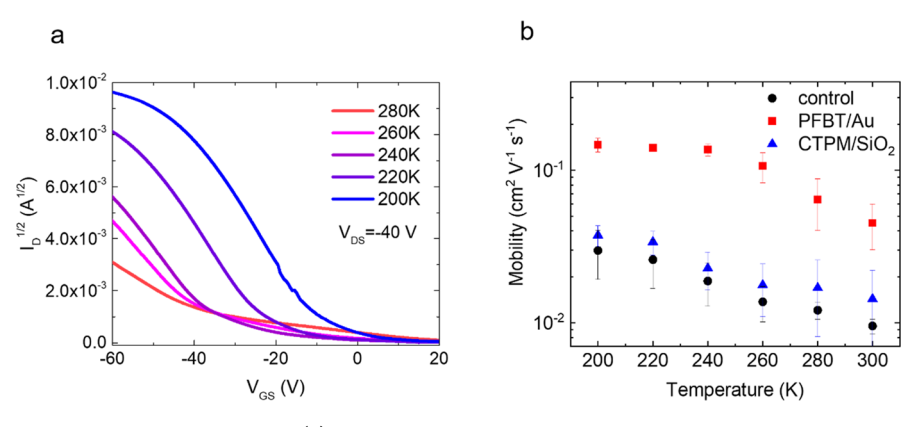


Figure 3. Electrical measurements of PEA_2SnI_4 devices. (a) Representative I-V curves at different temperatures for a PEA_2SnI_4 device with PFBT/Au source-drain contacts. (b) Field-effect mobility vs temperature for different device architectures.

but since the bottom-gate FET measurements adopted in this study probe the bottom, buried interface, we expect that charge transport here is less influenced by the roughness than it would be the case for top-gate devices.

The GIWAXS measurements (Figure 2d-f) confirmed that all the perovskite films were high quality and crystalline in nature. The X-ray diffraction patterns are similar in Figure 2d,e indicating that a similar structure is adopted in the control and PFBT/Au samples. Note that the control film on untreated Au yielded a similar pattern as the control on untreated SiO₂. These reflections are present in the X-ray diffraction pattern in Figure 2f also, suggesting that this structure is also present in the CTPM/SiO₂ sample. The X-ray diffraction pattern in Figure 2f, however, contains additional reflections. This is most clearly seen in the out-of-plane direction, in which we observe new reflections at q = 0.4, 0.8, 1.2, and 1.6 Å⁻¹, where the latter reflections are likely the higher-order reflections of the primary reflection at $q = 0.4 \text{ Å}^{-1}$. The presence of these reflections could suggest a population of grains having a different out-ofplane orientation; it could similarly suggest the presence of a different polymorph not observed in the control or the PFBT/ Au samples. Assuming the latter, this new phase is likely also monoclinic with lattice parameters equivalent to the crystal structure reported by Takahashi et al. 45 We thus infer that, unlike the adsorption of PFBT on Au, adsorption of CTPM on SiO₂ can alter the structuring of the subsequently deposited perovskite, by either inducing a second preferential out-ofplane orientation or a second polymorph.

Based on the information gained on the structure and morphology of the films, we can now explain the differences observed in transistor characteristics. In the absence of major morphological and structural differences between the control and the PFBT/Au samples, the higher value of the roomtemperature mobility in the FETs with PFBT-treated contacts stems from improved injection guaranteed by the higher-workfunction electrode upon PFBT treatment. Charges generated at the contact must tunnel through or around the energetic injection barrier arising from the mismatch between the work function of the source electrode and the HOMO level of the semiconductor (or LUMO in the case of an n-type FET). SAM treatment of the electrodes provides an effective and versatile way of tuning the electrode work function by altering the local electric field at the surface of the contact due to the internal SAM dipole, thus reducing this energy barrier. The strength and orientation of SAM molecular dipole orientation dictates the magnitude of the shift, with the packing density playing a

critical role. An extensive discussion on this topic can be found in a recent review. ¹⁹ For the cased of PFBT, the internal dipoles in the SAM molecule can shift the work function by 0.2 to 0.5 eV, depending on the quality of the SAM layer. ^{46–49} Other factors will also contribute to this effect, as we will discuss later. The minor difference in mobility between the control and CTPM/SiO₂ devices, which are characterized by similar injection properties, could originate from the occurrence of a different orientation or the presence of a new phase in the latter. On the other hand, these differences are so small that they might simply reflect sample-to-sample variations.

Temperature-dependent charge transport measurements are common methods to determine the conduction mechanism in semiconductors, since the specific details of the temperature dependence of the mobility allow to distinguish between the different well-established mechanisms. Figure 3 summarizes the temperature effects on the electrical properties of the three different types of PEA₂SnI₄ FET devices. In Figure 3a, we show examples of transfer curves at different temperatures; the current increases substantially as temperature decreases. This is in agreement with results reported for 3D perovskites and is attributed to the suppression of ion motion in the perovskite lattice as well as a decrease in thermally induced structural fluctuations and dynamical disorder in the perovskite. ^{50–53}

The room-temperature threshold voltage varies from negative in some devices to positive in devices where the ptype intrinsic doping is more severe. This doping is generated by the Sn vacancies that most likely are present in the films due to their low characteristic formation energy and/or by the spontaneous conversion of the bulk Sn⁴⁺ impurity ions from the SnI₂ precursor to Sn²⁺ to gain a higher thermodynamic stability. 54-56 The threshold voltage decreases as the temperature decreases, most likely due to the reduction in the ionic scattering. Small sample-to-sample variations have been observed due to the differences in sample quality and possibly the mechanical delamination and microstrain resulting from the mismatch in the coefficient of thermal expansions of the consecutive device layers. 57,58 Figure 3b shows the impact of temperature on the device mobility for each device type. The PFBT/Au devices displayed an increase in mobility as the temperature decreased, rising from an average of (4.5 ± 1.5) . 2 cm² V⁻¹ s⁻¹ at 300 K to an average of $(1.5 \pm 1.5) \cdot 10^{-1}$ cm² V⁻¹ s⁻¹ at 200 K. In the control devices, the mobility increased from (9.5 \pm 1.1)·10⁻³ cm² V⁻¹ s⁻¹ at 300 K to (3 \pm $1.1)\cdot 10^{-2}$ cm² V⁻¹ s⁻¹ at 200 K, and in the CTPM/SiO₂

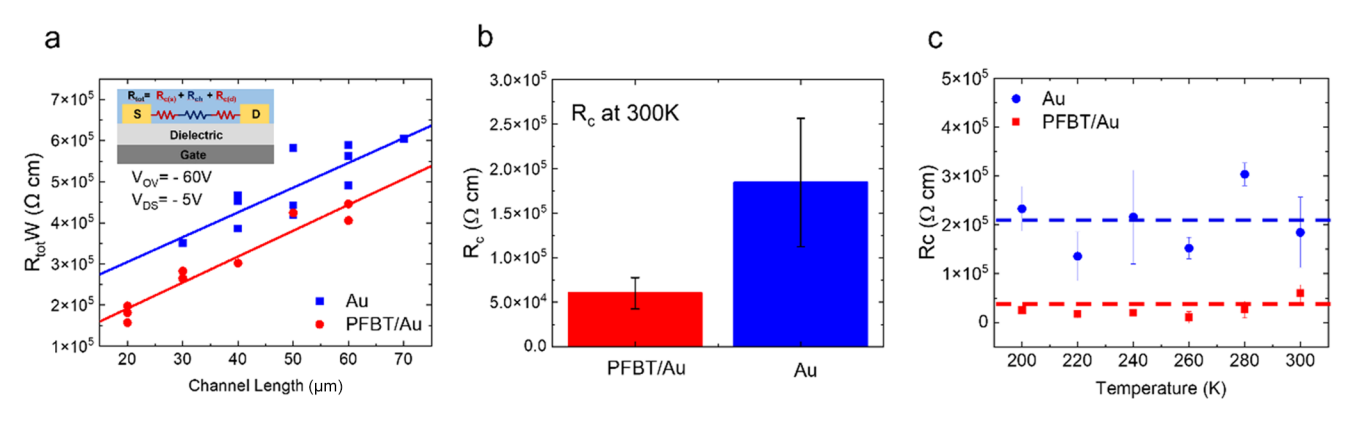


Figure 4. (a) Total device resistance vs channel length for bare Au (blue) and PFBT-treated Au (red) samples, with inset of device architecture. (b) R_c values of the Au (blue) and PFBT/Au samples (red) at room temperature. (c) Dependence of contact resistance on temperature in samples with treated (red) and untreated (blue) contacts.

devices, the mobility increased from $(1.4 \pm 0.8) \cdot 10^{-2}$ cm² V⁻¹ s^{-1} at 300 K to $(3.7 \pm 0.6) \cdot 10^{-2}$ cm² V⁻¹ s⁻¹ at 200 K. The $\mu(T)$ has a negative coefficient, similar to the case of the archetypal 3D perovskite methylammonium lead iodide (MAPI), 22,50,51 which has been assigned to the temperature dependence of the gate screening due to ionic motion and of the polarization disorder of the organic cation;²² however, in our samples, the increase in mobility with lowering the temperature is weaker than what was found previously in 3D perovskite FETs due to the fact that in the 2D layered structure the ion migration is less severe.³⁵ Nevertheless, an activated temperature dependence of the charge carrier mobility has been demonstrated even in 3D perovskites, namely in FETs based on mixed metal (Pb/Sn) perovskite, upon suppression of ion migration.¹³ Clearly, comparing the 3D and 2D perovskites in terms of temperature dependence of the electrical properties is very complex given the large number of parameters involved and our limited knowledge on the mechanism of charge transport in this emerging class of materials.

To deconvolute between the contributions of the channel (transport) and contacts (injection) to the temperature dependence of the device mobility, we evaluated the contact resistance in our FETs using the gated-TLM method.¹⁹ In this model, the total device resistance (R_{tot}) represents the sum between the channel resistance (R_{ch}) and contact resistance (R_c) , as shown in the inset in Figure 4a. By extrapolating the plots of R_{tot} vs channel length to L = 0, R_c is extracted. The corresponding curves for the case of untreated Au contacts and PFBT/Au contacts are shown in Figure 4a in blue and red, respectively, for a constant V_{DS} voltage of -5 V. In Figure 4b, we plot the average R_c obtained on three different device sets of each type at room temperature: $R_c = (1.84 \pm 0.72) \cdot 10^5 \Omega$ cm in devices with untreated contacts is over 3 times higher than that in the PFBT/Au devices, where $R_c = (5.9 \pm 1.7) \cdot 10^4$ Ω cm.

As expected, the contact properties of the CTPM/SiO₂ and the control samples are similar, since in both cases, the electrode is not functionalized; the data on the first is included in Figure 4 and for the latter in Figure S4.

The impact of PFBT treatment on contact resistance by increasing the work function of the electrode to reduce the Schottky barrier is well-documented. We do not exclude, however, the contribution of the perovskite layer mobility to the value of R_{cl} since the rate of injection from a contact

limited metal electrode is proportional to the semiconductor mobility.⁶⁰ We minimized this effect by focusing on coplanar devices. In order to ascertain the contribution of R_c to the temperature dependence of the mobility presented in Figure 3, we performed a similar gated-TLM analysis at each temperature investigated in this study; the evolution of contact resistance with temperature is shown in Figure 4c. We found that R_c does not show any notable dependence on temperature, indicating that the trend of $\mu(T)$ is governed by the changes in the properties within the channel as the temperature changes. A temperature-independent contact resistance might seem peculiar considering the theories of semiconductor transport. However, these theories only consider the electronic transport (p- or n-type) and are hence insufficient for describing charge injection in perovskites, where the ion motion is superimposed on the electronic transport. The Rc(T) dependence presented in Figure 4c arises from the competing effects of (i) an Arrhenius-like activated behavior arising from the shallow trap states that the carriers generated at the electrode must transit to reach the FET channel, counteracted by (ii) a negative temperature coefficient related to ionic motion. The first mechanism has been found in materials systems characterized by a purely electronic conduction, like organic semiconductors, 61 but the impact of ionic motion on contact resistance is still poorly understood. In this context, it is critical to recognize the significance of these findings: the migration of the ionic species within the perovskite layer does not only affect the channel mobility, as previously thought, but also the efficiency of the injection process through ion-hole scattering. This implies that freezing or, at least, reducing ion migration, would yield more efficient devices through the concerted increase in the intrinsic mobility of the semiconductor layer and a reduction in the parasitic contact resistance. Having established the evolution of the contact resistance with temperature, we can now better understand the variable temperature electrical measurements presented in Figure 3b. Similar to the case of contact resistance, the transport in the channel is a result of the thermally activated motion of holes due to the inherent shallow traps that are present in thin films, counteracted by interactions with the mobile ions which screen the gate field, thus reducing the apparent mobility by reducing the current.

To assess if the PFBT treatment introduces other effects that could lead to the reduction in R_{σ} we evaluated the chemical composition and the spatial distribution of the chemical

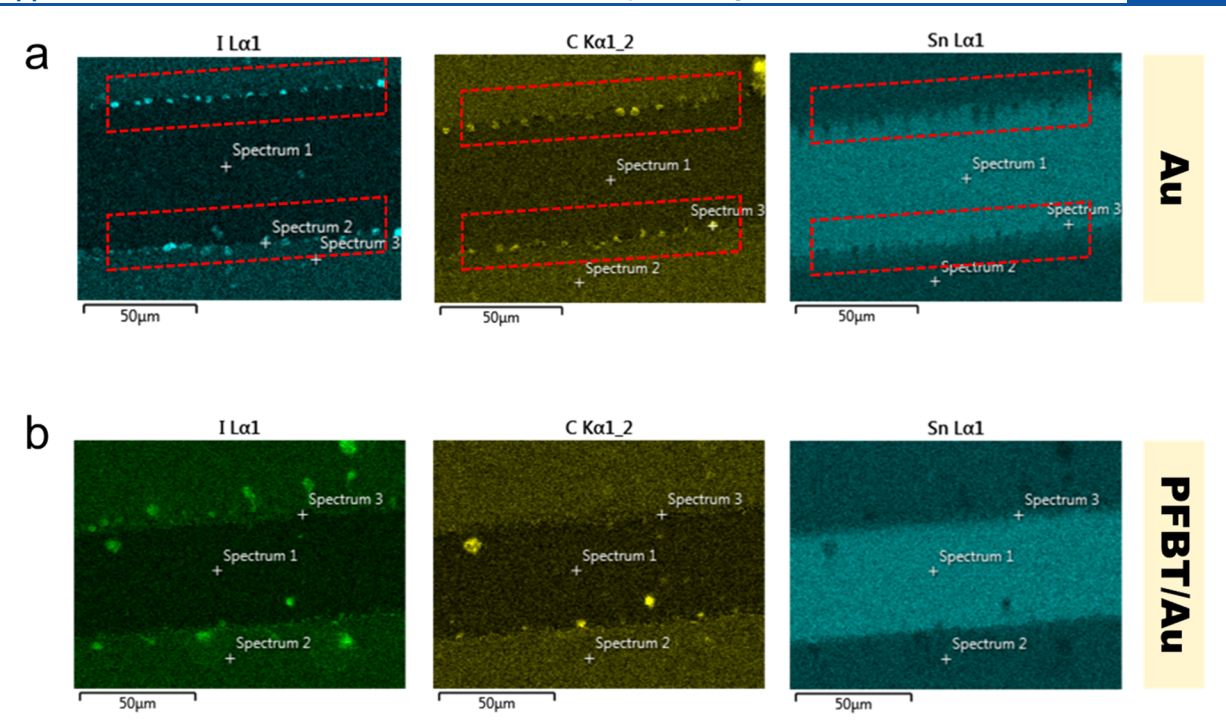


Figure 5. X-ray maps of samples showing elemental analysis of devices of (a) bare Au and (b) PFBT-treated Au. The edges of the channel and gold electrodes are highlighted in red. Bright regions in the X-ray maps show that carbon—iodine domains form at the edges on bare Au but not on Au coated with PFBT.

species in perovskite films deposited on Au and PFBT/Au by using SEM to acquire X-ray maps. In Figure 5, we show the results obtained from measurements performed on perovskite films deposited on bare Au and PFBT/Au substrates, respectively. These measurements confirm that in devices fabricated on untreated Au electrodes (Figures 5a and S5) uncontrolled chemical reactions occur at the edge of the Au electrode, generating domains rich in carbon-iodine and poor in tin at the interface between the channel and the electrodes (see the regions highlighted in red), which will contribute to the parasitic contact resistance. The nature of these species is still under investigation, but we do not exclude the formation of polyiodide melts from the interaction of the volatile I₂ species and the phenethylammonium iodide (PEAI), which can react aggressively with gold even at room temperature,⁶² although we have not seen evidence for these compounds within the resolution of our measurements. On the contrary, the presence of the PFBT monolayer on the electrodes prevents the direct interaction between the perovskite layer and the Au surface and, in doing so, suppresses the reaction channels. PFBT treatment thus represents an efficient way to reduce contact resistance by both adjusting the work function of the metal electrode and by acting as a diffusion barrier between the perovskite and the Au, limiting interfacial chemical reactions. It is important to emphasize the importance of these findings in a more general context. Chemical reactions at metal/perovskite interfaces are quite common, even in the case of noble metals, and their impact on the performance and stability of devices can be catastrophic.⁶³ The halogen, halide, and other volatile species generated in the presence of humidity, oxygen, and/or light even in encapsulated films can diffuse to the electrodes, leaving behind vacancies in the perovskite layer, causing the corrosion of the metal and, in some cases, the formation of redox couples with the perovskite. 16,64-66 The metal particles have also been

found to diffuse into the perovskite film under heat and/or light and react to produce metal halide species or other defect states. 67,68 The electrochemical reactions between the gold electrodes and mobile halogen species are accelerated under external biasing and the introduction of different buffer layers has been proposed to prevent these reactions. 27,31,69,70 The reduction in the injection barrier due to the intrinsic SAM dipoles and the inhibition of the interfacial reactions contribute to the lowering of the contact resistance in FETs with PFBTtreated contacts, as observed in Figure 4b, but separating between the two is difficult at the moment. Nevertheless, it is evident that the use of SAMs for contact modifications could play a pivotal role in the development of perovskite applications given the reduced complexity of the fabrication process and the fact that they allow great tunability of the electrode work function. Another advantage is that they yield a dense and continuous interlayer between the contact and the perovskite film, which inhibits the interaction between the highly volatile halide species and the metal, thus preventing the chemical reactions and carrier recombination. A downside, however, is that SAM treatment is limited to the bottom contacts, and different strategies should be developed for reducing the contact resistance in the case of top contacts. SAM treatment of electrodes thus enhances the device performance by both lowering the injection barrier and creating a buffer layer to inhibit the chemical reactions at the surface of the electrodes. Future work will establish how this treatment will impact the environmental and bias-stress stability of devices upon chemically tailoring the contacts with SAMs.

CONCLUSIONS

In summary, we systematically evaluated the physics of charge injection and transport in 2D perovskite FETs as a function of surface functionalization. We found that treatment of the contacts simultaneously assists with lowering of the charge injection barrier and inhibiting the chemical reactions that can occur at the electrode/perovskite interface between the metal and the ionic species reaching the surface of the perovskite layer. As a result, the contact resistance is reduced. The dielectric treatment does not significantly alter the device properties, suggesting that in these devices the processes taking place at the electrodes play a critical role in the transistor operation. The temperature dependence of the field-effect mobility resulted from the competition between the activated temperature behavior in the presence of electronic traps and the negative temperature coefficient due to ionic motion. Our results contribute to the fundamental understanding of the mechanism of charge injection in perovskite FETs and emphasize the importance of contact engineering in inhibiting the electrochemical reactions that occur at the surface of electrodes. These findings have implication for the development of other perovskite optoelectronic devices, where the effectiveness of charge injection is critical for device performance.

ASSOCIATED CONTENT

Supporting Information

The Supporting Information is available free of charge at https://pubs.acs.org/doi/10.1021/acsaelm.3c00149.

Example transfer curves obtained on different FET types; gated-TLM and SEM data (PDF)

AUTHOR INFORMATION

Corresponding Author

Oana D. Jurchescu — Department of Physics and Center for Functional Materials, Wake Forest University, Winston Salem, North Carolina 27109, United States; oocid.org/0000-0003-2204-2909; Email: jurchescu@wfu.edu

Authors

- Colin Tyznik Department of Physics and Center for Functional Materials, Wake Forest University, Winston Salem, North Carolina 27109, United States
- Matthew Waldrip Department of Physics and Center for Functional Materials, Wake Forest University, Winston Salem, North Carolina 27109, United States
- Ryan P. Sullivan Department of Physics and Center for Functional Materials, Wake Forest University, Winston Salem, North Carolina 27109, United States
- Motahhare Mirhosseini Department of Physics and Center for Functional Materials, Wake Forest University, Winston Salem, North Carolina 27109, United States
- Adam Berry Department of Chemical and Biological Engineering and Andlinger Center for Energy and the Environment, Princeton University, Princeton, New Jersey 08544, United States
- Sean Dwyer Department of Physics and Astronomy, Appalachian State University, Boone, North Carolina 28608, United States
- Hurriyet Yuce Cakir Department of Physics and Center for Functional Materials, Wake Forest University, Winston Salem, North Carolina 27109, United States
- Tonya Coffey Department of Physics and Astronomy, Appalachian State University, Boone, North Carolina 28608, United States

Yueh-Lin Loo — Department of Chemical and Biological Engineering, Princeton University, Princeton, New Jersey 08544, United States; orcid.org/0000-0002-4284-0847

Complete contact information is available at: https://pubs.acs.org/10.1021/acsaelm.3c00149

Notes

The authors declare no competing financial interest.

ACKNOWLEDGMENTS

The work at Wake Forest University was partially supported by the National Science Foundation under awards CMMI 2135937 and ECCS 1810273. The work at Princeton University was partially supported by NSF DMR-1627925.

REFERENCES

- (1) Green, M. A.; Ho-Baillie, A.; Snaith, H. J. The Emergence of Perovskite Solar Cells. *Nat. Photonics* **2014**, *8* (7), 506–514.
- (2) Correa-Baena, J. P.; Saliba, M.; Buonassisi, T.; Grätzel, M.; Abate, A.; Tress, W.; Hagfeldt, A. Promises and Challenges of Perovskite Solar Cells. *Science* **2017**, 358 (6364), 739–744.
- (3) Zhao, X.; Liu, T.; Loo, Y. L. Advancing 2D Perovskites for Efficient and Stable Solar Cells: Challenges and Opportunities. *Adv. Mater.* **2022**, *34*, 2105849.
- (4) Vaynzof, Y. The Future of Perovskite Photovoltaics—Thermal Evaporation or Solution Processing? *Adv. Energy Mater.* **2020**, *10* (48), 2003073.
- (5) Tsai, H.; Liu, F.; Shrestha, S.; Fernando, K.; Tretiak, S.; Scott, B.; Vo, D. T.; Strzalka, J.; Nie, W. A Sensitive and Robust Thin-Film x-Ray Detector Using 2D Layered Perovskite Diodes. *Sci. Adv.* **2020**, 6 (15), No. eaay0815.
- (6) Tsai, H.; Shrestha, S.; Pan, L.; Huang, H. H.; Strzalka, J.; Williams, D.; Wang, L.; Cao, L. R.; Nie, W. Quasi-2D Perovskite Crystalline Layers for Printable Direct Conversion X-Ray Imaging. *Adv. Mater.* **2022**, *34* (13), 2106498.
- (7) Tan, Z.; Moghaddam, R. S.; Lai, M. L.; Docampo, P.; Higler, R.; Deschler, F.; Price, M.; Sadhanala, A.; Pazos, L. M.; Credgington, D.; Hanusch, F.; Bein, T.; Snaith, H. J.; Friend, R. H. Bright Light-Emitting Diodes Based on Organometal Halide Perovskite. *Nat. Nanotechnol.* **2014**, *9* (9), 687–692.
- (8) Fakharuddin, A.; Gangishetty, M. K.; Abdi-Jalebi, M.; Chin, S. H.; bin Mohd Yusoff, A. R.; Congreve, D. N.; Tress, W.; Deschler, F.; Vasilopoulou, M.; Bolink, H. J. Perovskite Light-Emitting Diodes. *Nat. Electron.* **2022**, *5* (4), 203–216.
- (9) Paulus, F.; Tyznik, C.; Jurchescu, O. D.; Vaynzof, Y. Switched-On: Progress, Challenges, and Opportunities in Metal Halide Perovskite Transistors. *Adv. Funct. Mater.* **2021**, *31* (29), 2101029.
- (10) Lin, Y. H.; Pattanasattayavong, P.; Anthopoulos, T. D. Metal-Halide Perovskite Transistors for Printed Electronics: Challenges and Opportunities. *Adv. Mater.* **2017**, *29* (46), 1702838.
- (11) Liu, Y.; Chen, P. A.; Hu, Y. Recent Developments in Fabrication and Performance of Metal Halide Perovskite Field-Effect Transistors. *J. Mater. Chem. C* **2020**, 8 (47), 16691–16715.
- (12) Abiram, G.; Thanihaichelvan, M.; Ravirajan, P.; Velauthapillai, D. Review on Perovskite Semiconductor Field-Effect Transistors and Their Applications. *Nanomater.* **2022**, *12* (14), 2396.
- (13) Senanayak, S. P.; Dey, K.; Shivanna, R.; Li, W.; Ghosh, D.; Zhang, Y.; Roose, B.; Zelewski, S. J.; Andaji-Garmaroudi, Z.; Wood, W.; Tiwale, N.; MacManus-Driscoll, J. L.; Friend, R. H.; Stranks, S. D.; Sirringhaus, H. Charge Transport in Mixed Metal Halide Perovskite Semiconductors. *Nat. Mater.* 2023, 22 (2), 216–224.
- (14) Zhao, X.; Xu, H.; Wang, Z.; Lin, Y.; Liu, Y. Memristors with Organic-inorganic Halide Perovskites. *InfoMat* **2019**, *1*, 183–210.
- (15) Lei, L.; Dong, Q.; Gundogdu, K.; So, F. Metal Halide Perovskites for Laser Applications. *Adv. Funct. Mater.* **2021**, *31* (16), 2010144.

- (16) Boyd, C. C.; Cheacharoen, R.; Leijtens, T.; McGehee, M. D. Understanding Degradation Mechanisms and Improving Stability of Perovskite Photovoltaics. *Chem. Rev.* **2019**, *119* (5), 3418–3451.
- (17) Droseros, N.; Dänekamp, B.; Tsokkou, D.; Boix, P. P.; Banerji, N. Charge Injection and Trapping at Perovskite Interfaces with Organic Hole Transporting Materials of Different Ionization Energies. *APL Mater.* **2019**, 7 (4), No. 041115.
- (18) Goetz, K. P.; Vaynzof, Y. The Challenge of Making the Same Device Twice in Perovskite Photovoltaics. *ACS Energy Lett.* **2022**, 7 (5), 1750–1757.
- (19) Waldrip, M.; Jurchescu, O. D.; Gundlach, D. J.; Bittle, E. G. Contact Resistance in Organic Field-Effect Transistors: Conquering the Barrier. *Adv. Funct. Mater.* **2020**, *30* (20), 1904576.
- (20) Zeidell, A. M.; Tyznik, C.; Jennings, L.; Zhang, C.; Lee, H.; Guthold, M.; Vardeny, Z. V.; Jurchescu, O. D. Enhanced Charge Transport in Hybrid Perovskite Field-Effect Transistors via Microstructure Control. *Adv. Electron. Mater.* **2018**, 4 (12), 1800316.
- (21) Phung, N.; Al-Ashouri, A.; Meloni, S.; Mattoni, A.; Albrecht, S.; Unger, E. L.; Merdasa, A.; Abate, A. The Role of Grain Boundaries on Ionic Defect Migration in Metal Halide Perovskites. *Adv. Energy Mater.* **2020**, *10* (20), 1903735.
- (22) Senanayak, S. P.; Yang, B.; Thomas, T. H.; Giesbrecht, N.; Huang, W.; Gann, E.; Nair, B.; Goedel, K.; Guha, S.; Moya, X.; McNeill, C. R.; Docampo, P.; Sadhanala, A.; Friend, R. H.; Sirringhaus, H. Understanding Charge Transport in Lead Iodide Perovskite Thin-Film Field-Effect Transistors. *Sci. Adv.* **2017**, 3 (1), No. e1601935.
- (23) Khassaf, H.; Yadavalli, S. K.; Zhou, Y.; Padture, N. P.; Kingon, A. I. Effect of Grain Boundaries on Charge Transport in Methylammonium Lead Iodide Perovskite Thin Films. *J. Phys. Chem. C* 2019, 123 (9), 5321–5325.
- (24) Yu, W.; Li, F.; Yu, L.; Niazi, M. R.; Zou, Y.; Corzo, D.; Basu, A.; Ma, C.; Dey, S.; Tietze, M. L.; Buttner, U.; Wang, X.; Wang, Z.; Hedhili, M. N.; Guo, C.; Wu, T.; Amassian, A. Single Crystal Hybrid Perovskite Field-Effect Transistors. *Nat. Commun.* **2018**, *9*, 5354.
- (25) Matsushima, T.; Hwang, S.; Terakawa, S.; Fujihara, T.; Sandanayaka, A. S. D.; Qin, C.; Adachi, C. Intrinsic Carrier Transport Properties of Solution-Processed Organic—Inorganic Perovskite Films. *Appl. Phys. Express* **2017**, *10* (2), No. 024103.
- (26) Tang, L.; Peng, Y.; Zhou, Z.; Wu, Y.; Xu, J.; Li, J.; Du, Y.; Huang, L.; Cai, H.; Ni, J.; Zhang, J. High-Performance Organic—Inorganic Hybrid Perovskite Thin-Film Field-Effect Transistors. *Appl. Phys. A: Mater. Sci. Process.* **2018**, *124* (9), 624.
- (27) Peng, Y.; Tang, L.; Zhou, Z.; Xu, J.; Li, J.; Cai, H.; Ni, J.; Zhang, J. Enhancing Perovskite TFTs Performance by Optimizing the Interface Characteristics of Metal/Semiconductor Contact. *J. Phys. D. Appl. Phys.* **2018**, *51* (44), 445101.
- (28) Li, M. K.; Chen, T. P.; Lin, Y. F.; Raghavan, C. M.; Chen, W. L.; Yang, S. H.; Sankar, R.; Luo, C. W.; Chang, Y. M.; Chen, C. W. Intrinsic Carrier Transport of Phase-Pure Homologous 2D Organolead Halide Hybrid Perovskite Single Crystals. *Small* **2018**, *14* (52), 1803763.
- (29) Liu, F.; Wang, L.; Wang, J.; Wang, F.; Chen, Y.; Zhang, S.; Sun, H.; Liu, J.; Wang, G.; Hu, Y.; Jiang, C. 2D Ruddlesden Popper Perovskite Single Crystal Field-Effect Transistors. *Adv. Funct. Mater.* **2021**, *31* (1), 2005662.
- (30) Kerner, R. A.; Schulz, P.; Christians, J. A.; Dunfield, S. P.; Dou, B.; Zhao, L.; Teeter, G.; Berry, J. J.; Rand, B. P. Reactions at Noble Metal Contacts with Methylammonium Lead Triiodide Perovskites: Role of Underpotential Deposition and Electrochemistry. *APL Mater.* **2019**, *7* (4), No. 041103.
- (31) Wang, J.; Senanayak, S. P.; Liu, J.; Hu, Y.; Shi, Y.; Li, Z.; Zhang, C.; Yang, B.; Jiang, L.; Di, D.; Ievlev, A. V.; Ovchinnikova, O. S.; Ding, T.; Deng, H.; Tang, L.; Guo, Y.; Wang, J.; Xiao, K.; Venkateshvaran, D.; Jiang, L.; Zhu, D.; Sirringhaus, H. Investigation of Electrode Electrochemical Reactions in CH₃NH₃PbBr₃ Perovskite Single-Crystal Field-Effect Transistors. *Adv. Mater.* **2019**, *31* (35), 1902618. (32) Choi, K.; Choi, H.; Min, J.; Kim, T.; Kim, D.; Son, S. Y.; Kim, G. W.; Choi, J.; Park, T. A Short Review on Interface Engineering of

- Perovskite Solar Cells: A Self-Assembled Monolayer and Its Roles. Sol. RRL. 2020, 4 (2), 1900251.
- (33) Lee, J. Y.; Kim, S. Y.; Yoon, H. J. Small Molecule Approach to Passivate Undercoordinated Ions in Perovskite Light Emitting Diodes: Progress and Challenges. *Adv.Opt. Mater.* **2022**, *10* (1), 2101361.
- (34) Matsushima, T.; Hwang, S.; Sandanayaka, A. S. D.; Qin, C.; Terakawa, S.; Fujihara, T.; Yahiro, M.; Adachi, C. Solution-Processed Organic-Inorganic Perovskite Field-Effect Transistors with High Hole Mobilities. *Adv. Mater.* **2016**, *28* (46), 10275–10281.
- (35) Zhu, H.; Liu, A.; Shim, K. I.; Hong, J.; Han, J. W.; Noh, Y. Y. High-Performance and Reliable Lead-Free Layered-Perovskite Transistors. *Adv. Mater.* **2020**, 32 (31), 2002717.
- (36) Lamport, Z. A.; Barth, K. J.; Lee, H.; Gann, E.; Engmann, S.; Chen, H.; Guthold, M.; McCulloch, I.; Anthony, J. E.; Richter, L. J.; DeLongchamp, D. M.; Jurchescu, O. D. A Simple and Robust Approach to Reducing Contact Resistance in Organic Transistors. *Nat. Commun.* **2018**, *9* (1), 5130.
- (37) Ward, J. W.; Smith, H. L.; Zeidell, A.; Diemer, P. J.; Baker, S. R.; Lee, H.; Payne, M. M.; Anthony, J. E.; Guthold, M.; Jurchescu, O. D. Solution-Processed Organic and Halide Perovskite Transistors on Hydrophobic Surfaces. *ACS Appl. Mater. Interfaces* **2017**, *9* (21), 18120–18126.
- (38) Lamport, Z. A.; Broadnax, A. D.; Scharmann, B.; Bradford, R. W.; Delacourt, A.; Meyer, N.; Li, H.; Geyer, S. M.; Thonhauser, T.; Welker, M. E.; Jurchescu, O. D. Molecular Rectifiers on Silicon: High Performance by Enhancing Top-Electrode/Molecule Coupling. ACS Appl. Mater. Interfaces 2019, 11 (20), 18564–18570.
- (39) Sullivan, R. P.; Morningstar, J. T.; Castellanos-Trejo, E.; Bradford, R. W.; Hofstetter, Y. J.; Vaynzof, Y.; Welker, M. E.; Jurchescu, O. D. Intermolecular Charge Transfer Enhances the Performance of Molecular Rectifiers. *Sci. Adv.* **2022**, *8* (31), No. eabq7224.
- (40) Kagan, C. R.; Mitzi, D. B.; Dimitrakopoulos, C. D. Organic-Inorganic Hybrid Materials as Semiconducting Channels in Thin-Film Field-Effect Transistors. *Science* **1999**, 286 (5441), 945–947.
- (41) Lamport, Z. A.; Haneef, H. F.; Anand, S.; Waldrip, M.; Jurchescu, O. D. Tutorial: Organic Field-Effect Transistors: Materials, Structure and Operation. *J. Appl. Phys.* **2018**, *124* (7), No. 071101.
- (42) Choi, H. H.; Cho, K.; Frisbie, C. D.; Sirringhaus, H.; Podzorov, V. Critical Assessment of Charge Mobility Extraction in FETs. *Nat. Mater.* **2018**, *17*, 2–7.
- (43) Xu, K.; Sun, W.; Shao, Y.; Wei, F.; Zhang, X.; Wang, W.; Li, P. Recent Development of PeakForce Tapping Mode Atomic Force Microscopy and Its Applications on Nanoscience. *Nanotechnol. Rev.* **2018**, *7* (6), 605–621.
- (44) Diemer, P. J.; Lamport, Z. A.; Mei, Y.; Ward, J. W.; Goetz, K. P.; Li, W.; Payne, M. M.; Guthold, M.; Anthony, J. E.; Jurchescu, O. D. Quantitative Analysis of the Density of Trap States at the Semiconductor-Dielectric Interface in Organic Field-Effect Transistors. *Appl. Phys. Lett.* **2015**, *107* (10), 103303.
- (45) Takahashi, Y.; Obara, R.; Nakagawa, K.; Nakano, M.; Tokita, J.-Y.; Inabe, T. Tunable Charge Transport in Soluble Organic-Inorganic Hybrid Semiconductors. *Chem. Mater.* **2007**, *19* (25), 6312–6316.
- (46) Mei, Y.; Fogel, D.; Chen, J.; Ward, J. W.; Payne, M. M.; Anthony, J. E.; Jurchescu, O. D. Interface Engineering to Enhance Charge Injection and Transport in Solution-Deposited Organic Transistors. *Org. Electron.* **2017**, *50*, 100–105.
- (47) Ward, J. W.; Loth, M. A.; Kline, R. J.; Coll, M.; Ocal, C.; Anthony, J. E.; Jurchescu, O. D. Tailored Interfaces for Self-Patterning Organic Thin-Film Transistors. *J. Mater. Chem.* **2012**, 22, 19047—19053.
- (48) Lamport, Z. A.; Barth, K. J.; Lee, H.; Gann, E.; Engmann, S.; Chen, H.; Guthold, M.; McCulloch, I.; Anthony, J. E.; Richter, L. J.; DeLongchamp, D. M.; Jurchescu, O. D. A Simple and Robust Approach to Reducing Contact Resistance in Organic Transistors. *Nat. Commun.* 2018, *9*, 5130.
- (49) Choi, S.; Fuentes-Hernandez, C.; Wang, C. Y.; Khan, T. M.; Larrain, F. A.; Zhang, Y.; Barlow, S.; Marder, S. R.; Kippelen, B. A

Study on Reducing Contact Resistance in Solution-Processed Organic Field-Effect Transistors. *ACS Appl. Mater. Interfaces* **2016**, 8 (37), 24744–24752.

- (50) Labram, J. G.; Fabini, D. H.; Perry, E. E.; Lehner, A. J.; Wang, H.; Glaudell, A. M.; Wu, G.; Evans, H.; Buck, D.; Cotta, R.; Echegoyen, L.; Wudl, F.; Seshadri, R.; Chabinyc, M. L. Temperature-Dependent Polarization in Field-Effect Transport and Photovoltaic Measurements of Methylammonium Lead Iodide. *J. Phys. Chem. Lett.* **2015**, *6* (18), 3565–3571.
- (51) Chin, X. Y.; Cortecchia, D.; Yin, J.; Bruno, A.; Soci, C. Lead Iodide Perovskite Light-Emitting Field-Effect Transistor. *Nat. Commun.* **2015**, *6* (1), 7383.
- (52) Brenner, T. M.; Egger, D. A.; Rappe, A. M.; Kronik, L.; Hodes, G.; Cahen, D. Are Mobilities in Hybrid Organic—Inorganic Halide Perovskites Actually "High"? *J. Phys. Chem. Lett.* **2015**, 6 (23), 4754–4757.
- (53) Senanayak, S. P.; Abdi-Jalebi, M.; Kamboj, V. S.; Carey, R.; Shivanna, R.; Tian, T.; Schweicher, G.; Wang, J.; Giesbrecht, N.; Di Nuzzo, D.; Beere, H. E.; Docampo, P.; Ritchie, D. A.; Fairen-Jimenez, D.; Friend, R. H.; Sirringhaus, H. A General Approach for Hysteresis-Free, Operationally Stable Metal Halide Perovskite Field-Effect Transistors. *Sci. Adv.* **2020**, *6* (15), eaaz4948.
- (54) Dey, K.; Roose, B.; Stranks, S. D. Optoelectronic Properties of Low-Bandgap Halide Perovskites for Solar Cell Applications. *Adv. Mater.* **2021**, 33 (40), 2102300.
- (55) Ricciarelli, D.; Meggiolaro, D.; Ambrosio, F.; De Angelis, F. Instability of Tin Iodide Perovskites: Bulk p-Doping versus Surface Tin Oxidation. *ACS Energy Lett.* **2020**, *5* (9), 2787–2795.
- (56) Meggiolaro, D.; Ricciarelli, D.; Alasmari, A. A.; Alasmary, F. A. S.; De Angelis, F. Tin versus Lead Redox Chemistry Modulates Charge Trapping and Self-Doping in Tin/Lead Iodide Perovskites. *J. Phys. Chem. Lett.* **2020**, *11* (9), 3546–3556.
- (57) Mei, Y.; Diemer, P. J.; Niazi, M. R.; Hallani, R. K.; Jarolimek, K.; Day, C. S.; Risko, C.; Anthony, J. E.; Amassian, A.; Jurchescu, O. D. Crossover from Band-like to Thermally Activated Charge Transport in Organic Transistors Due to Strain-Induced Traps. *Proc. Natl. Acad. Sci. U. S. A.* **2017**, *114* (33), E6739–E6748.
- (58) Lin, H.; Zhang, Z.; Zhang, H.; Lin, K. Te; Wen, X.; Liang, Y.; Fu, Y.; Lau, A. K. T.; Ma, T.; Qiu, C. W.; Jia, B. Engineering van Der Waals Materials for Advanced Metaphotonics. *Chem. Rev.* **2022**, *122* (19), 15204–15355.
- (59) Mei, Y.; Fogel, D.; Chen, J.; Ward, J. W.; Payne, M. M.; Anthony, J. E.; Jurchescu, O. D. Interface Engineering to Enhance Charge Injection and Transport in Solution-Deposited Organic Transistors. *Org. Electron.* **2017**, *50*, 100–105.
- (60) Scott, J. C.; Malliaras, G. G. Charge Injection and Recombination at the Metal-Organic Interface. *Chem. Phys. Lett.* **1999**, 299 (2), 115–119.
- (61) Pesavento, P. V.; Puntambekar, K. P.; Frisbie, C. D.; McKeen, J. C.; Ruden, P. P. Film and Contact Resistance in Pentacene Thin-Film Transistors: Dependence on Film Thickness, Electrode Geometry, and Correlation with Hole Mobility. *J. Appl. Phys.* **2006**, *99* (9), No. 094504.
- (62) Shlenskaya, N. N.; Belich, N. A.; Grätzel, M.; Goodilin, E. A.; Tarasov, A. B. Light-Induced Reactivity of Gold and Hybrid Perovskite as a New Possible Degradation Mechanism in Perovskite Solar Cells. J. Mater. Chem. A 2018, 6 (4), 1780–1786.
- (63) Boyd, C. C.; Cheacharoen, R.; Leijtens, T.; McGehee, M. D. Understanding Degradation Mechanisms and Improving Stability of Perovskite Photovoltaics. *Chem. Rev.* **2019**, *119* (5), 3418–3451.
- (64) Kar, S.; Kaushal, K.; Yantara, N.; Mhaisalkar, S. G. Optical Simulations in Perovskite Devices: A Critical Analysis. *ACS Photonics* **2022**, 9 (10), 3196–3214.
- (65) Bi, J.; Zhang, J.; Giannakou, P.; Wickramanayake, T.; Yao, X.; Wang, M.; Liu, X.; Shkunov, M.; Zhang, W.; Zhao, Y. A Highly Integrated Flexible Photo-Rechargeable System Based on Stable Ultrahigh-Rate Quasi-Solid-State Zinc-Ion Micro-Batteries and Perovskite Solar Cells. *Energy Storage Mater.* **2022**, *51*, 239–248.

- (66) Kerner, R. A.; Schulz, P.; Christians, J. A.; Dunfield, S. P.; Dou, B.; Zhao, L.; Teeter, G.; Berry, J. J.; Rand, B. P. Reactions at Noble Metal Contacts with Methylammonium Lead Triiodide Perovskites: Role of Underpotential Deposition and Electrochemistry. *APL Mater.* **2019**, *7* (4), No. 041103.
- (67) Zhu, J.; Liu, Z.; Hu, P.; Guo, M.; Li, Y.; Li, J.; Akram, M. A.; Wei, M. Grain Boundary Passivation Using D131 Organic Dye Molecule for Efficient and Thermally Stable Perovskite Solar Cells. ACS Sustain. Chem. Eng. 2022, 10 (41), 13825–13834.
- (68) Sakhatskyi, K.; John, R. A.; Guerrero, A.; Tsarev, S.; Sabisch, S.; Das, T.; Matt, G. J.; Yakunin, S.; Cherniukh, I.; Kotyrba, M.; Berezovska, Y.; Bodnarchuk, M. I.; Chakraborty, S.; Bisquert, J.; Kovalenko, M. V. Assessing the Drawbacks and Benefits of Ion Migration in Lead Halide Perovskites. *ACS Energy Lett.* **2022**, *7* (10), 3401–3414.
- (69) Song, Y.; Li, L.; Hao, M.; Bi, W.; Wang, A.; Kang, Y.; Li, H.; Li, X.; Fang, Y.; Yang, D.; Dong, Q. Elimination of Interfacial-Electrochemical-Reaction-Induced Polarization in Perovskite Single Crystals for Ultrasensitive and Stable X-Ray Detector Arrays. *Adv. Mater.* **2021**, 33 (52), 2103078.
- (70) Tang, L.; Peng, Y.; Zhou, Z.; Wu, Y.; Xu, J.; Li, J.; Du, Y.; Huang, L.; Cai, H.; Ni, J.; Zhang, J. High-Performance Organic-Inorganic Hybrid Perovskite Thin-Film Field-Effect Transistors. *Appl. Phys. A: Mater. Sci. Process.* **2018**, *124*, 624.

☐ Recommended by ACS

Ion Migration Induced Unusual Charge Transport in Tin Halide Perovskites

Taewan Roh, Yong-Young Noh, et al.

JANUARY 13, 2023 ACS ENERGY LETTERS

READ 🗹

Effects of Ti Doping on the Electrical Properties and Gate-Bias Stability of Amorphous Zinc-Tin-Oxide Thin-Film Transistors

Sunghyun Park, Yong-Hoon Kim, et al.

MAY 30, 2023

ACS APPLIED ELECTRONIC MATERIALS

READ

Voltage Bias Stress Effects and Electronic Stability of π -Conjugated Crosslinked Tin Halide Perovskites

Laura Flannery, Luisa Whittaker-Brooks, et al.

NOVEMBER 22, 2022

ACS APPLIED ENERGY MATERIALS

RFAD **[**✓

Defect Reconfiguration in Hole-Doped PbSe via Minute Te Doping for Significantly Enhanced Thermoelectric Performance

Jinchang Sun, Gangjian Tan, et al.

FEBRUARY 13, 2023

ACS APPLIED ENERGY MATERIALS

READ 🗹

Get More Suggestions >